Opto-Electronics Review

Effect of Al₂O₃ decoration on the opto-electrical properties of a porous Si/Cr₂O₃ composite

M. Ghrib[a,b*] , B. Tlili[c], M. Razeg[a], R. Ouertani[a], M. Gaidi[d,e], H. Ezzaouia[a]

[a]Laboratory of Semiconductor Nanostructures and Advanced Technologies (LASNTA),
Research Centre and Energy Technologies, Borj-Cédria, Tunisia
[b]Higher Institute of Environmental Sciences and Technologies of Borj-Cédria (ISSTE)
[c]University of Tunis El Manar, National School of Engineers Tunis, LR-11-ES19 Laboratory
of Applied Mechanics and Engineering (LR-MAI), 1002 Tunis, Tunisia
[d]Laboratoire de Photovoltaïque, Centre de Recherches et des Technologies de l'Energie,
Technopole de Borj-Cédria, BP 95, 2050 Hammam-Lif, Tunisia
[e]Department of Applied Physics and Astronomy, University of Sharjah,
PO Box 27272, Sharjah, United Arab Emirates Sharjah

Article info	Abstract
	In this work, we present an extensive investigation of the effect of Al₂O₃ decoration on the morphological, structural and opto-electronic properties of a porous Si (Sip)/Cr₂O₃ composite. The Sip layers were prepared by the anodization method. Al₂O₃ and Cr₂O₃ thin films were deposited by physical vapour deposition. The morphological and micro-structural properties of Sip/Cr₂O₃/Al₂O₃ were studied using the scanning electron microscope, energy dispersive X-ray spectroscopy and X-ray diffraction techniques. It was found that Al₂O₃ decoration with different concentration strongly affects the Sip/Cr₂O₃ microstructure mainly at the level of porosity. Variable angle spectroscopic ellipsometry demonstrates a strong correlation between optical constants (*n* and *k*) of Sip/Cr₂O₃/Al₂O₃ and microstructure properties. Dielectric properties of Sip/Cr₂O₃/Al₂O₃ such as electrical conductivity and conduction mechanism were explored using impedance spectroscopy over the temperature interval ranging from 340 to 410°C. A semiconductor to the metallic transition has been observed at high frequency.

1. Introduction

Metal oxides such as TiO₂, ZrO₂, SnO₂, SiO₂, Al₂O₃ and Cr₂O₃ are very interesting materials applied in different high technological fields. These binary oxides are currently being investigated as potential SiO₂ substitutes in the next generations of semiconductor devices [1]. Among these materials, Cr₂O₃ thin films are of high importance for a wide variety of applications.

They have found potential uses in opto-electronic devices, mainly as radiation filter for solar energy harvesting [2,3], electrode for electro-chromic windows [4], and lithium batteries [5]. Cr₂O₃ thin films have demonstrated

excellent hardness along with high wear and corrosion resistance [6]. Alumina chromium catalysts based on the Cr₂O₃/Al₂O₃ binary system have been known for a long time and they are widely used in the reaction of dehydrogenation of light alkanes [7-10]. The properties of alumina chromium catalysts depend on numerous factors: method and regime of the support preparation, nature of the deposited component, and variety of the phase states and degree of dispersity [11-13]. When deposit on Sip/Cr₂O₃ alumina appears to be highly promising material because of its high electrical permittivity, a bandgap of about 2.98 eV [14,15] and its excellent thermal stability [16]. There are ample routes for the synthesis of Cr₂O₃ thin films such as laser ablation [17], e-beam evaporation [18], chemical and physical vapour deposition (PVD) [19,20, 21], and spray pyrolysis [22]. PVD is selected in this work

*Corresponding author:
mondher.gharib@isste.u-carthage.tn, mondher.ghrib@yahoo.fr

regarding too many advantages, such as large production area and uniform thickness distribution. Using suitable precursors and post-deposition treatments, PVD has ability to have a fine control over a concentration of deposited materials and oxygen vacancy [23]. Actually, the nature of active catalytic centres in the Al_2O_3/Cr_2O_3 binary system for the reaction of alkane dehydrogenation is not well known. The challenge of increasing the catalytic activity and decreasing the abrasive properties of the alumina chromium catalysts remains urgent. A detailed investigation of the electronic structure is necessary in order to solve these problems. Photoluminescence techniques (PL) are well known for their high sensitivity in comparison to the spectrophotometric investigation methods.

Their selectivity and non-disruptive action appear to be a promising direction for the investigation of samples with high chromium content (above 1.0 wt%), mainly the optoelectronic properties of the Al_2O_3/Cr_2O_3 system, in particular, Cr^{3+}: Al_2O_3 with chromium content up to 1.0 wt%. Many methods were developed to probe the local structures of a nano volume of Cr^{3+} that allowed differentiating phase states of the doped matrix and investigating the local electronic structure [24]. Spectroscopic ellipsometry (SE) [25] is an excellent technique used for the analysis of very thin layers. It has been used for the optoelectronic investigation of $Sip/Cr_2O_3/Al_2O_3$. Our samples structure has been modelled as alternately overlapping layers; each layer has its own intrinsic properties. The main purpose of this work is to study the influence of the Al_2O_3 content on Sip/Cr_2O_3 micro-structural and optoelectronic properties.

2. Experimental details

The porous Si layer has been prepared using electrochemical anodization technique. A current density of 10 mA/cm^2 has been applied to a silicon substrate immersed in hydrofluoric acid (HF) solution. The obtained Sip layer was then etched in an acidic mixing solution (HNO_3: 10%, HF: 20%, H_2O_2: 70%) followed by rinsing with distilled water and drying under oxygen to produce a Sip with an ordered pore structure. Using the PVD technique, we respectively deposited on the Sip substrate a layer of CrN. The Al_2O_3 films were then deposited with different concentrations: (a) 0%, (b) 3.5%, (c) 7%, (d) 11%, (e) 19%, (f) 24% relative to the concentration of CrN by an RF reactive magnetron sputtering at a deposition temperature of 660°C. The $Sip/CrN/Al_2O_3$ obtained structure was then thermally introduced into an oven under oxygen flow at a temperature equal to 1500°C to substitute nitrogen with oxygen and to convert CrN to Cr_2O_3.

3. Characterizations

The microstructure and elemental composition of the $Sip/Cr_2O_3/Al_2O_3$ samples were characterized using a FE-SEM (model ZEISS Ultra Plus) equipped with an EDX detector and at an accelerating voltage of 30 kV. The crystallographic structures of $Sip/Cr_2O_3/Al_2O_3$ were carried out by an X-ray diffraction (XRD) technique using a Bruker D8 advance X-ray diffractometer working with CuK_α radiation ($\lambda_{CuK\alpha}$ = 1.5406 Å).

A controlled HP4192A analyser operating in a frequency range between 7 Hz and 19 MHz was used to analyse the electrical properties of $Sip/Cr_2O_3/Al_2O_3$. An electrical test has been conducted using two electrodes configuration. The electrodes were deposited on both ends of the sample using silver paste. Electrical characterizations were carried out over a large range of temperature between 190-370°C and the frequency varied in the 5 Hz-13 MHz range.

4. Results and interpretation

4.1 Morphology and structure of $Sip/Cr_2O_3/Al_2O_3$

4.1.1 Energy dispersive X-ray (EDX) analysis

The film composition has been evaluated using EDX. Figure 1 shows the EDX spectrum of the $Sip/Cr_2O_3/Al_2O_3$ thin films and the relative elementary composition. EDX analysis confirms the presence of mainly Si, O, Al, and Cr in the $Sip/Cr_2O_3/Al_2O_3$ samples. The atomic percentage of Si, O, Cr, and Al is 45.8%, 31.8%, 12.0%, and 3.2%, respectively.
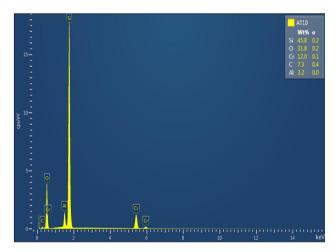

Fig. 1. The EDX analysis of $Sip/Cr_2O_3/Al_2O_3$

EDX surface mapping (Fig. 2) of $Sip/Cr_2O_3/Al_2O_3$ clearly shows a uniform distribution of all the elements throwing the whole surface.

4.1.2 SEM analysis

Figure 3 shows a cross section view of $Sip/Cr_2O_3/Al_2O_3$ layers after coating as a function of alumina concentration: (a) 0%, (b) 3.5%, (c) 7%, (d) 11%, (e) 19%, (f) 24% relative to the concentration of CrN.

In general, the growth of the layers begins with the incorporation of aluminium crystals in Sip/Cr_2O_3 pores. The material forms small pseudo -pyramids by nucleation [26,27]. The cross-section view shows the growth of a columnar layer where the thickness increases with an Al_2O_3 concentration.

4.1.3 X-ray diffraction analysis

Evolution of XRD spectra of $Sip/Cr_2O_3/Al_2O_3$ samples annealed at 660°C is presented in Fig. 4. The spectra show eight diffraction peaks corresponding respectively to SiO_2 [101], Al_2O_3 [104], Al_2O_3 [311], Al_2O_3 [200], Al_2O_3 [115], Cr_2O_3 [115], Cr_2O_3 [120], and Al_2O_3 [511]
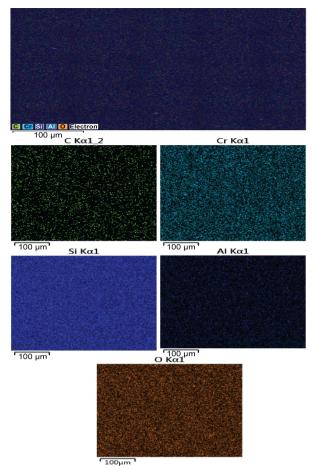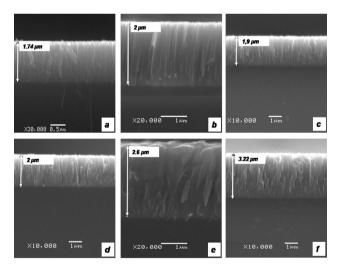
Fig. 2. The EDX-mapping of a Sip/Cr₂O₃/Al₂O₃ thin film.

Fig. 3. SEM cross-sectional images of Sip/Cr₂O₃ coated with Al₂O₃ at different concentration: (a) 0%, (b) 3.5%, (c) 7%, (d) 11%, (e) 19%, (f) 24%.

planes of cubic Si phase, with a preferential orientation along [101] direction. The integration of aluminium crystals in the pores of Si coated with Cr_2O_3 under oxygen flow gives rise to another phase of alumina, which appears at different orientations.

To calculate the average size of Al_2O_3 crystallites, the Debye Scherrer equation has been used following the equation below [28]:

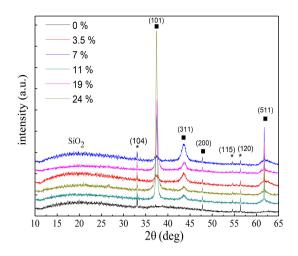$$D = \frac{0.9\lambda}{\beta 2 \cos\theta} \,, \qquad (1)$$

Fig.4. X-ray diffraction patterns of Sip/Cr₂O₃ coated with Al₂O₃ at different concentration.

where D is the average crystallite size, λ is the wavelength of the X -rays, θ is the Bragg diffraction angle, and β is the adjusted FWHM. The Al_2O_3 crystallites size increases from 2.8 nm to 6.7 nm as the Al_2O_3 concentration increases. The increase in the size of the crystallites was probably due to a diffusion of aluminium crystals from the surface towards the interior of the Sip coated with Cr_2O_3, which improved the crystallinity of the structure of the films.

4.2 Opto-electrical characterization

4.2.1 Optical analysis

The analysis of ellipsometric spectra requires the use of an optical model fitting exactly the configuration of the surface studied.

This will allow us to determine the optical parameters with good precision. For this purpose, samples were considered as a multilayer, consisting of a succession of layers of different compositions as shown in Fig. 5. The compositions of each layer were reported in Table 1.

Our proposed model is in harmony with De Laet *et al*. [29,30]. Based on the approximation of the effective medium (EMMA) of Bruggeman [31] it is shown by our model in Fig. 5. It can be noticed that there are five layers superimposed vertically (layer 1 - layer 5).
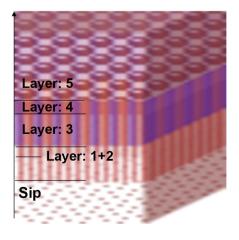

Fig. 5. Ellipsometric model of the multilayer structure Sip/Cr₂O₃/Al₂O₃./Al₂O₃.

Table 1.
Layer thicknesses and film porosity at different concentration of Al$_2$O$_3$.

Al$_2$O$_3$ concentration (%)	Layer 1+2 Al$_2$O$_3$+Cr$_2$O$_3$ (nm)	Layer 3 Al$_2$O$_3$+Cr$_2$O$_3$ (nm)	Layer 4 Al$_2$O$_3$+Cr$_2$O$_3$ (nm)	Layer 5 Al$_2$O$_3$ (nm)	Porosity (%)	RMSE
0 %	®	®	®	®	82	0.019
3.5 %	82	28	37	13	73	0.028
7 %	50	12	22	16	65	0.037
11 %	46	13	24	17	55	0.046
19 %	200	120	190	90	37	0.073
24 %	220	130	160	110	20	0.09

The proposed structure is composed of vacuum mixtures, Cr$_2$O$_3$, Si, and Al$_2$O$_3$, but each layer has intrinsic compositions. The optical model is accepted when the unbiased estimator, which is the root means squared error (RMSE) is under 9% [32].

$$RMSE = \sqrt{\frac{1}{2N-P-1}\sum_{j=1}^{N}\left[\left(tan\,\psi_j^m - tan\,\psi_j^s\right)^2 + \left(cos\,\Delta_j^m - cos\,\Delta_j^s\right)^2\right]}. \tag{2}$$

Determination of the physical parameters (n and k) depends on the adequate optical model to fit the tan ψ and cos Δ experimental data. The constructed optical model of the multilayer structure is schematized in Fig. 5. Where Ψ and Δ denote the amplitude ratio and phase difference, respectively, between the p-polarization and s-polarization components of the polarization state of the incident light, or the so-called ellipsometric parameters. N is the number of points, P is the number of parameters, m refers to the measured spectra and s refers to the simulated spectra.

After any optimization, we have obtained a good adjustment between the experimental results and theory fit (Fig. 6). The curves exhibit an almost close agreement throughout the spectral range. This method can also be used to determine the thickness of the studied layer based on the interference between the reflected rays.

In Table 1 the layer thickness and the RMSE values corresponding were recorded. The optical constants, such as the refractive index (n) and the extinction coefficient (k) were extracted and evaluated as a function of the Al$_2$O$_3$ (Fig. 7).

The refractive index n has been found to increase with the Al$_2$O$_3$ concentration, while the extinction coefficient k decreases. For example, at 600 nm the refractive index increases from 2 to 3.5 while the extinction coefficient decreases. This behaviour can be attributed to the diffusion of cations along the grain boundaries of Al$_2$O$_3$ which
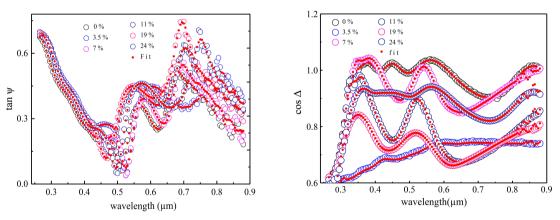

Fig. 6. Experimentally measured (symbols) and fitted (red dots) spectroscopic ellipsometry data of Sip/Cr$_2$O$_3$ coated with Al$_2$O$_3$ at different concentration.
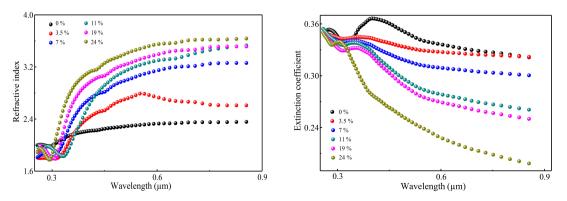

Fig. 7. Effect of Al$_2$O$_3$ concentration on the refractive index n and the extinction coefficient k of Sip/Cr$_2$O$_3$/Al$_2$O$_3$

creates an opposite flow of vacancies towards the surface of the Sip/Cr_2O_3 layer. The vacancies can condense and, then, reach the Cr_2O_3/Al_2O_3 interface to form cavities under the grain boundaries of Al_2O_3.

4.2.2 Conductivity measurements

The complex impedance diagrams measured on all the $Sip/Cr2O3/Al2O3$ samples over a frequency range (100 Hz to 13 MHz), and temperature (300-410°C), are shown in the representation of Nyquist [$Z'' = f(Z')$] in Fig. 8. In practice, it is possible to find several contributions to a dielectric response of an oxidized material (grains, grain boundaries, interface, etc.). The semicircles corresponding to $Sip/Cr_2O_3/Al_2O_3$ show different radii (unsimilar to Debye). This effect is explained by a dipolar system involving multi-relaxation processes [33] and indicating the semiconductor nature of all the samples. This also indicates a change in the resistance R_0 as a function of the deposited alumina concentrations. Variation in the peak Z″ intensity confirms the presence of a low-capacity semiconductor region that we can associate with the response of the Cr_2O_3 grain embedded in alumina, and of the vacuum percentage changing from sample to sample.

Others pay attention to a variation in the radii of the semicircle of each sample.

4.2.3 Imaginary part of impedance

The graphs showing the evolution of the imaginary part Z″ of the impedance of the $Sip/Cr_2O_3/Al_2O_3$ sample with frequency at different temperatures are shown in Fig. 8. Maximum of Z″ gives the frequency f_{max} relaxations which are governed by the Arrhenius [34-37] law:

$$f_{max} = f_0 e^{\frac{E_{a(z'')}}{k_B T}} . \qquad (3)$$

Where $E_{a(Z'')}$ is the activation energy and f_0 is the characteristic phonon frequency and k_B is the Boltzmann constant.

The activation energy associated with the relaxation process $E_{a(Z'')}$ was determined from Eq. (3) by the plotting log(f_{max}) vs. reciprocal of temperature. We note in Table 2 that the activation energy increases with alumina content to 2.31 eV, with an Al_2O_3 concentration equal to 19% and decreases thereafter.
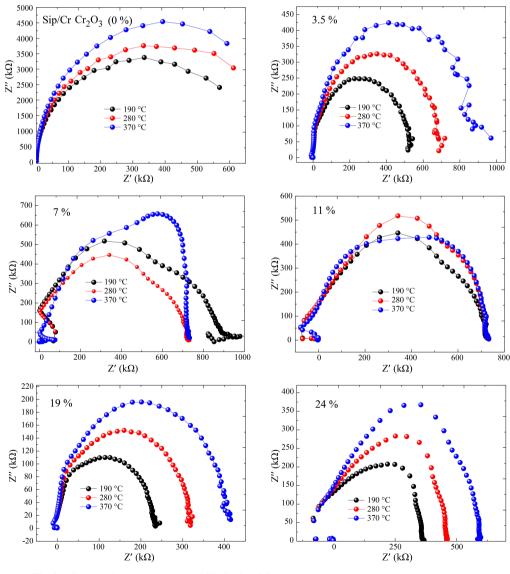

Fig. 8. Complex impedance spectra of $Sip/Cr_2O_3/Al_2O_3$.

Table 2.
Activation energy E_a and barrier height W_m of Sip/Cr$_2$O$_3$/Al$_2$O$_3$

Al$_2$O$_3$ conc.	$E_{a(Z'')}$ (eV)	$E_{a(dc)}$ (eV)	W_m (eV)
a	1.91	1.82	1.55
b	1.99	1.86	1.65
c	2	1.89	1.68
d	2.2	1.93	1.73
e	2.31	2.08	1.81
f	1.79	1.79	1.64

The observed variation is explained by the incorporation of Al$_2$O$_3$ in Sip/Cr$_2$O$_3$, and the decrease in the vacuum percentage, which facilitates the rate of jump activated thermally. The decrease in $E_{a(Z'')}$ for [Al$_2$O$_3$] equal to 24% is probably due to the nucleation of a new surface layer which Al$_2$O$_3$ crystals are very far apart which ceases the thermally activated jump [38]. This evolution could also be attributed to vacancies in deposited alumina and to interface defects due to vacancies in chromium occupied by oxygen atoms after the surface coating with Al$_2$O$_3$. The values of $E_{a(Z'')}$ for Sip/Cr$_2$O$_3$/Al$_2$O$_3$ (Fig. 9) show two domains of activation energy with temperature.

Change in the electrical properties of the prepared thin film can be explained by the presence of a new oxide formed in the pores of Si by transfer of the oxygen supplied

during the external oxide dissociation. One cause of the oxide dissociation is the excess of cations created at the grain boundaries, subsequently causing them to diffuse through the layer. Conductivity follows power law with the pulsation given by the equation below [39]:

$$\sigma_t = \sigma_{dc} + \sigma_{ac}(T, \omega), \qquad (4)$$

where ω is the angular frequency, T is the absolute temperature, σ_{dc} is the independent frequency conductivity or dc conductivity and σ_{ac} is the ac conductivity.

4.2.4   Frequency dependence of ac conductivity

In order to determine the conduction mechanism of dispersions of Sip/Cr$_2$O$_3$/Al$_2$O$_3$, we have calculated the conductivity values of dispersions over the frequency range [1 Hz, 10 Hz] and at different temperatures in Fig. 10.

Dependence of the alternative conductivity σ_{ac} with frequency at different temperatures can be modelled by Jonscher's universal power law:

$$\sigma_{ac} = A\omega^s . \qquad (5)$$

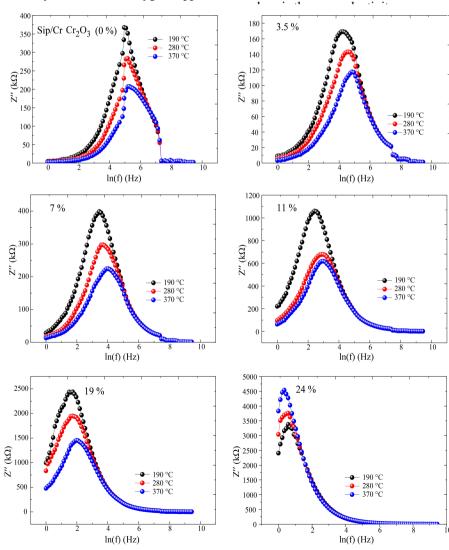A is the constant dependent on temperature, s is the material property which can have any value between 0 and 1,

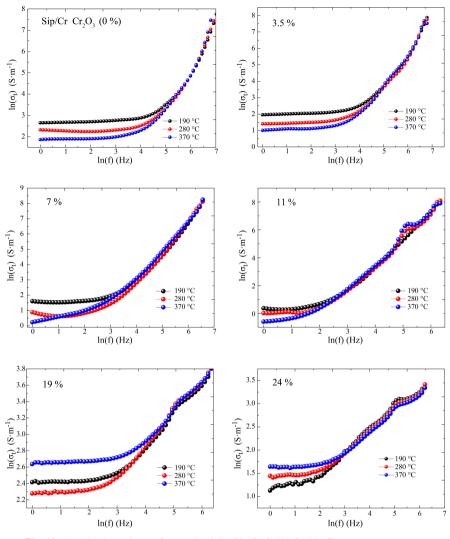**Fig. 9.**   Angular dependance of Sip/Cr$_2$O$_3$/Al$_2$O$_3$.

Fig. 10. Angular dependance of ac conductivity Sip/Cr₂O₃/Al₂O₃ thin films.

The evolution of *s* with temperature is dependent on the conduction mechanism. The exponent "*s*" expresses the relative reduction in the size of alumina crystals with frequency and is defined as follows:

$$s = \frac{d \ln \sigma_{ac}}{d \ln \omega} . \qquad (6)$$

However, the frequency exponent *s* raised from the slope of $\ln(\sigma_t)$ [Fig. 11(a)] decreases proportionally with

temperature. These results can be explained by the charge transfer, which has been described as a superposition of the various conduction phenomena. Sip/Cr₂O₃/Al₂O₃ morphology contains metal islands surrounded by amorphous alumina regions. Electronic wave functions are localized in amorphous regions but delocalized in metallic regions. For the charge transfer, metal conduction takes place in the metal islands while it is done by jumping in the amorphous regions. Inside the metal region, there is inter-
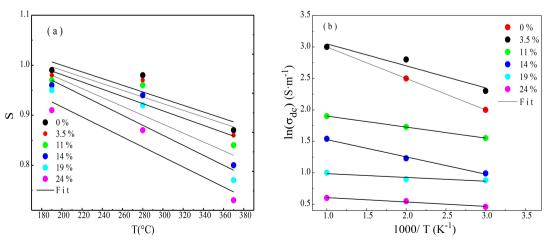

Fig. 11. (a) Temperature dependence of the exponent *s* and (b) dc conductivity curve for Sip/Cr₂O₃/Al₂O₃. The dots are the experimental points and the solid line is the least-square straight line fit.

fibrillar and intra-fibrillar conduction by hopping loads from the end of a chain to the other. The equation correlated with the model is written as follows [40]:

$$S = 1 - \frac{6k_B T}{W_m}. \qquad (7)$$

T is the absolute temperature, W_m and k_B are respectively, the maximum height of the barrier and the Boltzmann constant. The value of W_m (Table 2) is determined from the adaptation of s as $1 - \frac{6k_B}{W_m} T$.

It can be noted that W_m increases slightly depending on the concentration of Al_2O_3 up to 1.81 eV, then decreases slightly.

Using the Arrhenius law to exploit the experimental results of dc conductivity [41]:

$$\sigma_{dc} = \frac{C}{T} e^{-\frac{E_{a(dc)}}{k_B T}}, \qquad (8)$$

where C is the constant and E_a is the activation energy for the hopping conduction.

Figure 11(b) shows the plot of $\ln(\sigma_{dc} \cdot T)$ *vs.* $1000/T$ for $Sip/Cr_2O_3/Al_2O_3$ thin films. It is observed that the films dc conductivity decreases when temperature increases according to Arrhenius law. This evolution demonstrates the thermal activation mechanism of the electrical conduction, which indicates a semiconductor's behaviour of the $Sip/Cr_2O_3/Al_2O_3$ hybrid system.

The activation energy $E_{a(dc)}$ is extracted from the slope of $\ln(\sigma_{dc} \cdot T)$ *vs.* $1000/T$. $E_{a(dc)}$ values are summarised in Table 2. Our electrical studies show that in thermal fluctuation it is possible to supply sufficient energy to a dipole hopping across the potential barrier from one position to another equilibrium position [42-44].

5. Conclusions

We have studied the opto-electrical properties of a Cr_2O_3/Al_2O_3 deposit in a porous silicon layer. It was found that the structural properties depend significantly on the Al_2O_3 concentration. From the XRD study, we note that the concentration of Al_2O_3 deposited on Sip/Cr_2O_3 was a key factor in improving crystallinity. After the deposition of Al_2O_3 under oxygen on Sip/Cr_2O_3 the structure tends to crystallize for a temperature which reaches 660°C. The ellipsometric analysis of $Sip/Cr_2O_3/Al_2O_3$ shows the evolution of optical properties (refractive index, extinction coefficient) as a function of the Al_2O_3 concentration. Consequently, the refractive index increases while the extinction coefficient decreases with the concentration of Al_2O_3. This change appears to be linked to the progressive increase in the pores filling as a function of Al_2O_3 concentration and structure modification. In addition, from the impedance measurements, we note that the ac conductivity obeys the law of universal power and the transport of charge carriers can be quantified using the CBH model. Finally, these results are very interesting because we have successfully prepared films for opto-electronic applications.

References

[1] Stesmansa, A. & Afanasev, V. V. Paramagnetic defects in annealed ultrathin layers of SiOx, Al₂O₃, and ZrO₂ on (100) Si. *Appl. Phys. Lett.* **85**, 17 (2004). http://dx.doi.org/10.1063/1.1787152

[2] Hutchins, M. G. Selective thin film coatings for the conversion of solar radiation. *Surf. Coat. Tech*. **20**, 301–320 (1983). http://dx.doi.org/10.1016/0376-4583(83)90111-5

[3] Geotti-Bianchini, F., Guglielmi, M., Polato, P. & Soraru, G. D. Preparation and characterization of Fe, Cr and Co oxide films on flat glass from gels. *J. Non. Cryst. Solids* **63**, 251–259 (1984). http://dx.doi.org/10.1016/0022-3093(84)90404-6

[4] Schuster, A. P., Nguyen, D. & Caporaletti, O. Solid state electrochromic infrared switchable windows. *Sol. Energy Mater.* **13**, 153–160 (1986). http://dx.doi.org/10.1016/0165-1633(86)90041-9

[5] Koksbang, R. & Norby, P. Reversibility of the electrochemical lithium insertion in Cr₃O₈ comparison with LiCr₃O₈. *Electrochim. Acta* **36**, 127–133 (1991). http://dx.doi.org/10.1016/0013-4686(91)85189-E

[6] Pang, X. *et al.* Annealing effects on microstructure and mechanical properties of chromium oxide coatings. *Thin Solid Films* **516,** 4685–4689 (2008). http://dx.doi.org/10.1016/j.tsf.2007.08.083

[7] Weckhuysen, B. & Schoonheydt, R. Alkanedehy, rogenation over supported chromium oxide catalysts. *Catal. Today* **417,** 223–232 (1999). http://dx.doi.org/10.1016/S0920-5861(99)00047-4

[8] Puurunen, R. & Weckhuysen, B. Spectroscopic study on the irreversible deactivation of chromia alumina dehydrogenation catalysts. *J. Catal.* **210**, 418–430 (2002). http://dx.doi.org/10.1016/j.ces.2004.07.103

[9] Gaspar, A., Brito, J. & Dieguez, L. Characterization of chromium species in catalysts for dehydrogenation and polymerization. *Mol. Catal. A. Chem*. **203**, 251266 (2003). http://dx.doi.org/10.1016/S1381-1169(03)00381-9

[10] PeiLi, P., ZhongLang, W., Luan, K. XiYan, L. & JunGuo, Y. The promotion effects of Ni on the properties of Cr/Al catalysts for propane dehydrogenation reaction. *Appl. Catal. A. Gen.* **522**, 172–179 (2016). http://dx.doi.org/10.1016/j.apcata.2016.05.007

[11] Nemykina, E. I. *et al.* Effect of chromium content on the properties of a microspherical alumina-chromium catalyst for isobutane dehydrogenation prepared with the use of a centrifugal thermal activation product of gibbsite. *Kinet. Catal.* **51**, 898–906 (2010). http://dx.doi.org/10.1134/S0023158410060169

[12] Nable, Y. C., Suib, S. L. & Galasso , F. S. Metal organic chemical vapour deposition of Al₂O₃ and Cr₂O₃ on nickel as oxidation barriers. *Surf. Coat. Tech*. **186**, 423–430 (2004). http://dx.doi.org/10.1016/j.surfcoat.2003.11.022

[13] Nemykina, E. I. *et al.* Effect of chromium content on the proper ties of a microspherical alumina chromium catalyst for isobutane dehydrogenation prepared with the use of a centrifugal thermal activation product of gibbsite. *Kinet. Catal.* **51**, 898–906 (2010). http://dx.doi.org/10.1134/S0023158410060169

[14] Yuzheng, G., Stewart, C. & Robertson, J. J. Electronic and magnetic properties of Ti₂O₃, Cr₂O₃, and Fe₂O₃ calculated by the screened exchange hybrid density functional. *J. Phys. Condens. Matter.* **24**, 1–8 (2012). http://dx.doi.org/10.1088/0953-8984/24/32/325504

[15] Holt, A. & Kofstad, P. Electrical conductivity and defect structure of Cr2O3. I. High temperatures (>1000°C), *Solid State Ion*. **69**, 127–136 (1994). http://dx.doi.org/10.1016/0167-2738(94)90401-4

[16] Dehouche, Z. *et al.* Cycling and thermal stability of nanostructured MgH2–Cr2O3 composite for hydrogen storage. *J. Alloy. Compound*. **347**, 31932 (2002). http://dx.doi.org/10.1016/S0925-8388(02)00784-3

[17] Sousa, P. M., Silvestre, A. J. & Conde, O. Cr₂O₃ thin films grown at room temperature by low pressure laser chemical vapour deposition. *Thin Solid Films* 519, 36533657 (2011). http://dx.doi.org/10.1016/j.tsf.2011.01.382

[18] Bagmut, A. G. *et al.* Morphology and conjunction of nanocrystals growing in Cr-O and V-O amorphous films during annealing. *Russian Phys. J.* **50**, 1071–1078 (2007). http://dx.doi.org/10.1007/s11182-007-0157-6

[19] Borisov, P. A., Hochstrat, V. V., Shvartsman, W., Kleemann, T., Eimüller, A. & Rodrguez, F. Thin Cr₂O₃ Films for Magneto electric Data storage deposited by Reactive E-beam Evaporation. *Ferroelectr. Lett. Sect.* **70**, 147–152 (2008). http://dx.doi.org/10.1080/00150190802384518

[20] Levchuk, D., Koch, F., Maier, H. & Bolt, H. Deuterium permeation through Eurofer and a-alumina coated Eurofer. *J. Nucl. Mater.* **328**, 1036 (2004). http://dx.doi.org/10.1016/j.jnucmat.2004.03.008

[21] Koch, F. *et al.* Crystallization behaviour of arc-deposited ceramic barrier coatings. *J. Nucl. Mater.* **140**, 3–29 (2004). http://dx.doi.org/10.1016/j.jnucmat.2004.04.206

[22] Misho, R. H., Murad, W. A. & Fattahallah, G. H. Preparation and optical properties of thin films of CrO$_3$ and Cr$_2$O$_3$ prepared by the method of chemical spray pyrolysis. *Thin Solid Films* **169**, 235–239 (1989). http://dx.doi.org/10.1016/0040-6090(89)90706-2

[23] Vepřek, S. Plasma-induced and plasma-assisted chemical vapour deposition. *Thin Solid Films* **130**, 135–154 (1985). http://dx.doi.org/10.1016/0040-6090(85)90303-7

[24] YiWu, S., Ning, H. & Dong, W. Investigations on the local structures of Cr^{3+}(3d^3) and Nd^{3+}(4f^3) ions at the trigonal Bi^{3+} sites in Bi$_4$Ge$_3$O$_{12}$. *Opt. Mater.* **28**, 1095–1100 (2006). http://dx.doi.org/10.1016/j.optmat.2005.06.010

[25] Ghrib, M. *et al.* Morphological and optical properties changes in nanocrystalline Si (nc-Si) deposited on porous aluminum nanostructures by plasma enhanced chemical vapour deposition for Solar energy applications. *Appl. Surf. Sci.* **257**, 9129-9134 (2011). http://dx.doi.org/10.1016/j.apsusc.2011.05.113

[26] Chayen, N. E., Saridakis, E., El-Bahar, Y. & Nemirovsky, R. Porous silicon: an effective nucleation-inducing material for protein crystallization. *J. Mol. Biol.* **312**, 591–595 (2001). http://dx.doi.org/10.1006/jmbi.2001.4995

[27] Kluth, O. *et al.* Modified Thornton model for magnetron sputtered zinc oxide,film structure and etching behaviour. *Thin Solid Films* **442**, 80–85 (2003). http://dx.doi.org/10.1016/s0040-6090(03)00949-0

[28] Cullity, B. D. & Stock, S. R. *Elements of X-Ray Diffraction*. 3rd edn (Prentice Hall, Upper Saddle River, New Jersey, 2001).

[29] De Laet, J., Terryn, H. & Vereecken, J. Development of an optical model for steady state porous anodic films on aluminium formed in phosphoric acid *Thin Solid Films* **320**, 241–252 (1998). http://dx.doi.org/10.1016/S0040-6090(97)00741-4

[30] Huang, G. S., Wu, X. L., Siu, G. G. & Chu, P. K. On the origin of light emission from porous anodic alumina formed in sulfuric acid. *Solid State Commun.* **137**, 621–624 (2006). http://dx.doi.org/10.1016/j.ssc.2006.01.005

[31] Puranik, S. M., & Mehrotra, S. C. Static permittivity of binary mixtures using an improved bruggeman model. *J. Mol. Liq.* **59**, 173–177 (1994). http://dx.doi.org/10.1016/0167-7322(93)00665-6

[32] Petrik, P. *et al.* Methods for optical modelling and cross-checking in ellipsometry and scatterometry. in *Proc. SPIE Optical Metrology,* vol. 9526 (2015). http://dx.doi.org/10.1117/12.2184833

[33] Khamzin, A. A., Nigmatullin, R. R. & Popo, I. I. Microscopic model of a non-Debye dielectric relaxation, The Cole-Cole law and its generalization. *Theor. Math. Phys.* **173**, 1604–1619 (2012). http://dx.doi.org/10.1007/s11232-012-0135-1

[34] Badapanda, T. *et al.* Frequency and temperature dependence dielectric study of strontium modified Barium Zirconium Titanate ceramics obtained by mechanochemical synthesis. *J .Mater. Sci Mater. Electron.* **26**, 3069–3082 (2015) http://dx.doi.org/10.1007/s10854-015-2799-4

[35] Stern, H. *et al.* Vibronically coherent ultrafast triplet-pair formation and subsequent thermally activated dissociation control efficient endothermic singlet fission. *Nat. Chem.* **9**, 1205–1212 (2017). http://dx.doi.org/10.1038/nchem.2856

[36] Liu, Q., Peng, M., Shen, B., Hu, B. & Chen, Q. Polymer chain diffusion and Li+ hopping of poly(ethylene oxide)/LiAsF6 crystalline polymer electrolytes as studied by solid state NMR and ac impedance. *Solid State Ion.* **255**, 74-79 (2014). http://dx.doi.org/.10.1016/j.ssi.2013.11.053

[37] Sharma, H. *et al.* Ac electrical conductivity and magnetic properties of BiFeO3–CoFe2O4 nanocomposites. *J. Alloy. Compd.* **599**, 32–33 (2014). http://dx.doi.org/ 10.1016/j.jallcom.2014.02.024

[38] Yassin, Y. A., Raouf, M., Abdelghany, A. M. & Abdelrazek, E. M. Enhancement of dielectric properties and AC electrical conductivity of nanocomposite using poly (vinyl chloride-co-vinyl acetate-co-2-hydroxypropyl acrylate) filled with graphene oxide. *J. Mater. Sci. Electron.* **29**, 15931–15945 (2018). http://dx.doi.org/10.1007/s10854-018-9679-7

[39] Hayat, M., Rafiq, S. K., Durrani , M. M. & Hasan, A. Impedancespectroscopy and investigation of conduction mechanism in BaMnO$_3$ nanorods. *Physica B*, *Condensed Matter*. **406**, 309–314, (2011). http://dx.doi.org/ 10.1016/j.physb.2010.09.026

[40] Ngai, K. L., Jonscher, A. K. & White, C. T. On the origin of the universal dielectric response. *Condens. Matter. Phys.* **277**, 185–189 (1979). http://dx.doi.org/10.1038/277185a0

[41] Belin, R., Zerouale, A., Pradel, A. & Ribes, M. Ion dynamics in the argyrodite compound Ag$_7$GeSe$_5$I, non-Arrhenius behaviour and complete conductivity spectra. *Solid State Ion.* **143**, 445–455 (2001). http://dx.doi.org/ 10.1016/S0167-2738(01)00883-9

[42] Saravanan, S., Anantharaman,. M. R. & Venkatachalam, V. Structural and electrical studies on tetrameric cobalt phthalocyanine and polyaniline composites. *Mater. Sci. Eng. B* **135**, 113–119 (2006). http://dx.doi.org/10.1016/j.mseb.2006.08.048

[43] Boughalmi, R., Boukhachem, A., Kahlaoui, M., Maghraoui, H. & Amlouk,. M. Physical investigations on Sb$_2$S$_3$ sprayed thin film for optoelectronic applications. *Mater. Sci. Semicond. Process*. **26**, 593–602 (2014). http://dx.doi.org/10.1016/j.mssp.2014.05.059

[44] Ouni ,B. *et al.* Investigation of electrical and dielectric properties of antimony oxide (Sb$_2$O$_4$) semiconductor thin films for TCO and optoelectronic applications. *J. Non-Crys. Solids* **36**7, 1–7 (2013). http://dx.doi.org/10.1016/j.jnoncrysol.2013.02.006